Journal of Nuclear Medicine, published on November 30, 2018 as doi:10.2967/jnumed.118.208710

Does measurement of ^{18}F-fluoride metabolic flux improve response assessment of breast cancer bone metastases compared with standardised uptake values in ^{18}F-fluoride PET/CT?

Gurdip K Azad[1], Musib Siddique[1], Benjamin Taylor[2], Adrian Green[1], Jim O'Doherty[3,4], Joanna Gariani[5], Glen M Blake[1], Janine Mansi[2], Vicky Goh[1], Gary J.R Cook[1,3]

[1]Cancer Imaging Department, School of Biomedical Engineering and Imaging Sciences, King's College London, St Thomas' Hospital, London, UK.

[2]Department of Oncology, Guys and St Thomas' Hospital NHS Foundation Trust, London, UK.

[3]King's College London & Guy's and St Thomas' PET Centre, St Thomas' Hospital, London, UK.

[4]Department of Molecular Imaging, Sidra Medicine, Doha, Qatar.

[5]Geneva University Hospitals, Rue Gabrielle-Perret-Gentil 4, 1205 Geneva, Switzerland.

First author: Dr Gurdip K Azad; Research Fellow

Address: Department of Cancer Imaging, KCL Division of Imaging Sciences & Biomedical Engineering

Lambeth Wing, St Thomas' Hospital, Westminster Bridge Road, London, SE1 7EH

Email: gurdip.azad@kcl.ac.uk

Tel No: +44 207 188 8364

Fax No: ++44 207 620 0790

Corresponding author: Gary Cook

Correspondence Address: Gary Cook, Clinical PET Centre, St Thomas' Hospital, Westminster Bridge Road, London, SE1 7EH, UK.

Email: gary.cook@kcl.ac.uk

Tel No: ++44 207 188 8364

Fax No: ++44 207 620 0790

Word Count: 4853

Short running title: ^{18}F-fluoride Ki, SUV and bone metastases

ABSTRACT

Purpose: To establish whether non-invasive measurement of changes in ^{18}F-fluoride metabolic flux to bone mineral (K_i) by positron emission tomography/ computed tomography (PET/CT) can provide incremental value in response assessment of bone metastases in breast cancer compared to maximum and mean standardized uptake values (SUV_{max}, SUV_{mean}).

Method: Twelve breast cancer patients starting endocrine treatment for de-novo or progressive bone metastases were included. Static ^{18}F-fluoride PET/CT scans were acquired 60 minutes post-injection, before and 8 weeks after commencing treatment. Venous blood samples were taken at 55 and 85 minutes post-injection to measure plasma ^{18}F-fluoride activity concentrations. This allowed calculation of K_i in individual bone metastases using a previously validated method. Percentage changes in K_i, SUV_{max} and SUV_{mean} were calculated from the same ≤ 5 index lesions from each patient. Clinical response up to 24 weeks, assessed in consensus by two experienced oncologists blinded to PET imaging findings, was used as a reference standard.

Results: In the 4 patients with clinical progressive disease (PD), mean K_i significantly increased (>25%) in all, SUV_{max} in 3 and SUV_{mean} in 2. In the 8 non-PD patients, K_i decreased or remained stable in 7, SUV_{max} in 5 and SUV_{mean} in 6. A significant mean percentage increase in K_i from baseline occurred in the 4 patients with PD compared with SUV_{max} and SUV_{mean} (89.7% vs 41.9% and 43.8%, respectively; $p<0.001$).

Conclusion: After 8 weeks of endocrine treatment for bone-predominant metastatic breast cancer, K_i more reliably differentiated PD from non-PD than SUV_{max} and SUV_{mean}, probably because measurement of SUVs underestimates fluoride clearance as changes in input function are not accounted for.

KEY WORDS

Breast cancer, bone metastases, heterogeneity, ^{18}Fluoride PET/CT.

INTRODUCTION

^{18}F-fluoride is a bone-specific tracer and a marker of osteoblast activity in metastatic bone deposits. Both sclerotic and lytic metastatic bone lesions are highly ^{18}F-fluoride avid *(1)* and show increased blood flow and metabolic flux (plasma clearance) to the bone mineral compartment (K_i), allowing quantification of the regional kinetics of abnormal bone metabolism on ^{18}F-fluoride positron emission tomography/computed tomography (PET/CT) *(2)*. K_i is related to histomorphometric measures of bone turnover (*3*,*4*) and its measurement by PET has been proposed as a valuable and feasible method for measuring changes in regional bone turnover as a result of treatment in skeletal metastases from breast cancer *(5)* and has also been evaluated in assessing response in bone metastases from prostate cancer (*6*). By taking account of delivery and extraction of ^{18}F-fluoride, K_i appeals as a more discriminatory parameter for assessing treatment response of bone metastases rather than static measures such as standardized uptake value (*7*,*8*). Although SUV is one of the commonest and simpler methods for quantifying ^{18}F-fluoride PET studies, requiring only a short static scan and thus averting the need for invasive arterial blood sampling and lengthy dynamic scans, regional delivery and metabolic activity may be affected by changes in tracer kinetics at other sites in the body, thus making K_i a potentially more accurate and discriminatory parameter as both the delivery (arterial input function) and local bone metabolism (time activity curve) are measured over time to calculate kinetic indices of local bone metabolism *(9,10)*.

Most quantitative ^{18}F-fluoride PET studies have been performed using 60-minute dynamic scans whereby the bone activity curve is combined with an arterial input function and K_i is calculated using Hawkins' three-compartmental model (*11-15*) or other simplified methods such as the Patlak method (*16-18*). However, only one dynamic scan can be acquired after a single injection of ^{18}F-fluoride with a limited field-of-view on the PET scanner, and the invasive nature of arterial blood sampling and the requirement of trained personnel makes this an unappealing procedure for routine use.

Different approaches that are simpler to implement, have been applied to avoid arterial cannulation (*19-22*) and allow multiple lesions to be measured (*23*). For example, a semi-population based input function (SBIF) method has previously been proposed whereby K_i is calculated by initially fitting a terminal exponential to the measurements of venous plasma concentrations and then adding a population-based residual curve (*24*). The main advantage of this methodology is to allow calculation of K_i from static ^{18}F-fluoride PET scans in multiple lesions

without the need for arterial sampling and allowing a more physiological measure of changes in bone turnover in response to treatment (*23*).

Previous osteoporosis studies have reported differences in SUVs and plasma clearance between cortical and trabecular bones suggesting different effects of treatment at different sites of the skeleton (*15*,*25*,*26*). One study reported a much higher mean percentage change in K_i than SUV (24% vs 3%) in the lumbar spine in osteoporotic women treated with teriparatide, suggesting potentially higher uptake of injected dose at other skeletal sites (*15*).

We hypothesized that measurement of K_i is feasible using a static method with venous blood measurements and K_i is more discriminatory than SUV_{max} and SUV_{mean} in treatment response assessment. The aim of this study was to compare ^{18}F-fluoride K_i derived from a static method (*27*) as well as SUV_{max} and SUV_{mean} in response assessment of breast cancer bone metastases to endocrine therapy and to determine the level of correlation between the two methods. We also aimed to evaluate the effect of endocrine therapy on K_i in non-metastatic cortical and trabecular sites in the skeleton.

MATERIALS AND METHODS

Participants

Twelve female breast cancer patients (mean age: 50.4 years, range: 40-79 years) with de-novo (n=5, 20 lesions) or progressive bone metastases (n=7, 52 lesions) starting endocrine treatment were included. Apart from 2 patients who had small volume lung and liver metastases, all other patients had bone-only disease. The endocrine treatments used were letrozole (n=7), tamoxifen (n=3), everolimus/exemestane (n=2). ^{18}F-fluoride PET/CT scans were acquired before and 8 weeks after starting treatment. Two experienced oncologists blinded to PET findings, determined clinical response (based on standard imaging including bone scans and CT; and clinical assessment, including pain scores as well as alkaline phosphatase and carcinoma antigen 15-3) up to 24 weeks after the start of treatment or until progression, whichever came first. This assessment was used as a reference standard. We categorized patients as either clinical progressive disease (PD) or non-progressive disease (non-PD). We chose to include and assess patients with partial response (PR) and stable disease (SD) together as non-PD as clinical management rarely differs in these 2 groups.

The study was approved by a Research Ethics Committee and the Administration of Radioactive Substances Advisory Committee and all patients signed an informed consent at the time of recruitment.

Blood Sampling

Venous blood samples (5 mL each) were acquired at 55 and 85 minutes post injection of ^{18}F-fluoride. Two 0.2 mL aliquots from each blood sample were weighed and then counted on a 10-sample well counter (2470 WIZARD2, PerkinElmer, London, UK), previously cross-calibrated with the PET scanner using a standard calibration technique subject to daily quality control. The calibration process used ^{18}F-FDG mixed with water in a 6 L phantom to a known activity concentration and scanned on the PET scanner. Ten 0.2ml samples were taken from the phantom and counted on the well counter for 3 minutes, allowing the calculation of a conversion factor between the scanner and well counter measured in counts per second (cps) per activity concentration (kBq/ml). Whole blood samples were then centrifuged for 5 minutes (6000 rpm), and two 0.2 mL samples of plasma from each were also weighed and then counted in the well counter. Resulting counts per minute were converted to activity concentrations (kBq/ml) using a calibration factor.

^{18}F-fluoride PET/CT Image Acquisition and Reconstruction

Intravenous injection of ^{18}F-fluoride (mean 228 ± 15 MBq) was performed, and scanning commenced after an uptake time of 60 minutes. Images were acquired from skull base to upper thighs with an axial field of view of 15.7 cm and an 11-slice overlap between bed positions, using a GE Discovery 710 PET/CT scanner (GE Healthcare, Chicago, USA). A low-dose CT scan (140 kV, 10 mA, 0.5 s rotation time, and 40 mm collimation) was performed at the start of imaging to provide attenuation correction and an anatomical reference. PET scan duration was set to 3 minutes per bed position.

PET image reconstruction included standard scanner-based corrections for radiotracer decay, scatter, randoms and dead-time. Emission sinograms were reconstructed with a time-of-flight ordered subset expectation maximization algorithm (2 iterations, 24 subsets), with a 256x256 matrix and a 4 mm full-width at half-maximum Gaussian post-reconstruction smoothing filter available from the manufacturer on the scanner front-end.

Image Analysis

On ^{18}F-fluoride PET/CT, we defined PD as a ≥ 25% increase in K_i, SUV_{max} or SUV_{mean}. Non-PD included partial responders (> 25% decrease in K_i, SUV_{max} or SUV_{mean}) and stable disease (<25% increase or decrease), adapted from European Organization for Research and Treatment of Cancer criteria, acknowledging these were originally described for ^{18}F-FDG (*28*).

Up to 5 of the hottest (SUV_{max} ≥10) (*29*) and largest (≥ 1cm) lesions were selected for analysis in each subject. SUV measurements were normalized to body weight. The lesion ROIs (regions of interest) were contoured on the static ^{18}F-fluoride PET/CT scans using in-house software. The ROIs were outlined semi-automatically using an initial 40% of maximum tumor pixel threshold around each metastasis followed by manual correction based on an oncologist and radiologist working in consensus. Tumor volumes were measured from the PET ROIs both at baseline and again at 8 weeks after starting treatment. The same ROIs were used to estimate K_i, SUV_{max} and SUV_{mean} in each lesion. K_i, SUV_{max} and SUV_{mean} values were also measured in non-metastatic trabecular (centre of L1 lumbar vertebra) and cortical (upper femoral shaft, 1cm below the lesser trochanter) bone similar to the metastatic ROIs. If L1 contained a metastasis then the nearest 'adjacent' normal vertebra was used as a non-metastatic trabecular ROI. No patients had metastatic disease in the subtrochanteric left femur.

K_i Analysis

Values of K_i in metastases were calculated from the static scan. Venous blood samples and a modified Patlak method of calculation was used as previously described by Siddique et al. *(27,30)* by using an input function obtained by adding a population residual curve to the exponential, obtained from the two venous blood samples taken 55 and 85 min after injection. The population arterial input function was acquired from 10 postmenopausal women as previously described *(19)* and also described in supplemental data.

K_i, SUV_{max} and SUV_{mean} at baseline and 8 weeks, percentage (%) change in K_i, SUV_{max} and SUV_{mean} from baseline (in patients with PD and non-PD) were used for statistical analyses.

Statistical Analysis

Changes in K_i, SUV_{max} and SUV_{mean} were expressed as a percentage change from baseline. Data that were normally distributed were expressed as a mean and standard deviation and compared using the paired t-test and data that were not normally distributed were log transformed first allowing a normal distribution**.** Correlations between the changes in K_i against SUV_{max} and SUV_{mean} were evaluated using Pearson correlation coefficient (*r*). For all statistical tests, a P value of ≤ 0.05 was considered statistically significant.

RESULTS

By the clinical reference standard, there were 4 patients with clinical PD (20 lesions) and 8 with non-PD (32 lesions). The values of K_i, SUV_{max} and SUV_{mean} (12 patients, 52 lesions) at baseline, 8 weeks (same 52 lesions) and % change in K_i, SUV_{max} and SUV_{mean} are shown in Table1 [and supplemental data].

Correlations were present between K_i and SUV_{max} and K_i and SUV_{mean} at baseline {r=0.632 (p<0.001), r=0.784 (p<0.001), respectively} and at 8 weeks {(r=0.830, p<0.001), (r=0.901, p<0.001), respectively} (Table 2).

A statistically significant correlation was observed overall between the % changes in K_i against % changes in SUV_{max} and SUV_{mean} at 8 weeks {r=0.852 (p<0.001), 0.901 (p<0.001), respectively} (Fig. 1) (Table 2) and also between % changes in K_i and SUV_{max} (r=0.811, p<0.001) and K_i and SUV_{mean} (0.904, p<0.001) in PD patients; and between K_i and SUV_{max} (r=0.863, p<0.001) and K_i and SUV_{mean} (r=0.933, p<0.001) in non-PD patients (Table 2). A correlation was noted between mean % change in K_i against SUV_{max} (r=0.88, p<0.001) and SUV_{mean} (r=0.81, p=0.001) in all patients (Fig. 2).

Measurements of K_i after 8 weeks of endocrine therapy showed a significant change in metastases from baseline with an overall mean % increase in K_i of 34.9% (SD=58.4) compared with 16.1% (SD=32.4) increase in SUV_{max} (p=0.005) and 17.5% (SD=35.7) in SUV_{mean} (p=0.001) (Table 1). In patients with PD, the mean % increase in K_i was 89.7% (SD=61.7) compared with 41.9% in SUV_{max} (SD=27.8) (p=0.001) and 43.8% (SD=41.9) in SUV_{mean} (p<0.001). In non-PD patients, the mean % increase in K_i was 10.7% (SD=36.7) compared with a mean % increase in SUV_{max} of 6.3% (SD=28.9) (p=0.60) and an increase in SUV_{mean} of 7.7% (SD=27.5) (p=0.70). The mean % increase in K_i was statistically significantly higher in patients with PD than non-PD {K_i=89.7% vs 10.7% (p<0.01) but not with SUV_{max} 41.9% vs 6.3% (p=0.067) or SUV_{mean}=43.8% vs 7.7% (p=0.153)} (Table 3).

On a per lesion basis, K_i increased by >25% in 15 out of 20 (75%), SUV_{max} in 11 out of 20 (55%) (p=0.13) and SUV_{mean} in 8 out of 20 (40%) lesions (p=0.13 and 0.02, respectively) in patients with clinical PD. K_i, SUV_{max} and SUV_{mean} decreased or remained stable in 27 out of 32 (84%) lesions in patients with clinical non-PD. K_i, SUV_{max} and SUV_{mean} were falsely positive (increased > 25%) in 5 of the 32 lesions in patients with clinical non-PD.

On a per patient basis, of the 4 patients with clinical PD, a mean % change in K_i correctly identified all 4 patients, a mean % change in SUV_{max} in 3 out of 4, and a mean % change in SUV_{mean} in 2 out of 4. In 8 patients with clinical non-PD, a % change in K_i accurately identified 7, a % change in SUV_{max} identified 5 and a % change in SUV_{mean} identified 6 out of 8 patients. K_i was falsely positive in 1, SUV_{max} in 3 and SUV_{mean} in 2 of the 8 patients.

The mean % change in K_i was 7.9 times higher in patients with high disease burden (n=7); > 5 bone metastases) than those with low disease burden (n=5) {mean K_i = 48.8% vs 6.2% (p=0.017). There was no significant difference in the mean SUV_{max} {18.6% vs 10.9%, p=0.22)} or mean SUV_{mean} {20.3% vs 11.7%, p=0.12} between the 2 groups.

The % change in K_i in normal cortical and trabecular non-metastatic bone were 21.7% vs -1.9%, respectively; the percentage change in SUV_{max} was 4.8% vs -12.6%, respectively and the % change in SUV_{mean} was -0.7% vs -17.1%, respectively. There was a statistically significant difference in K_i between baseline and 8-week values for cortical bone (p=0.018) and SUV_{max} between baseline and 8 weeks for trabecular bone (p=0.050), but other differences were not significant.

DISCUSSION

To our knowledge, this is the first study reporting an advantage in measuring changes in metabolic flux (plasma clearance) of ^{18}F-fluoride to bone mineral (K_i) as an early 8 week treatment response marker for breast cancer bone metastases compared to the static semi-quantitative measures SUV_{max} and SUV_{mean}. The methodology used, allows estimation of the arterial input function by correcting a population input function from venous plasma measurements. Together with measurements from a static PET acquisition at 60 minutes post injection, K_i can be estimated in any lesion within the static field of view *(27)*.

We observed expected correlations between K_i and SUV parameters at baseline, 8 weeks and between % change in K_i with % change in SUV parameters in patients with PD or non-PD.

Compared to a clinical reference standard using data up to 24 weeks, % change in K_i at 8 weeks correctly predicted PD in more patients and more lesions than either SUV_{max} or SUV_{mean} (4,3,2/4; 15,11,8/20, respectively) in patients with bone-predominant breast cancer undergoing endocrine treatment. K_i correctly predicted non-PD in more patients than SUV_{max} and SUV_{mean} (7,5,6/8, respectively) but no difference was observed on a per lesion basis. The mean percentage increase in K_i was statistically significantly higher in patients with PD than non-PD.

Metabolic flux of ^{18}F-fluoride provides an assessment of the local bone mineralization taking into account the availability of tracer (i.e. input function), whereas measurements of SUV ignore possible changes in the input function. In circumstances where plasma ^{18}F-fluoride concentration is reduced, either because of high global avidity of metastatic lesions or an increase in the metabolic activity of the remaining normal skeleton, then SUV parameters may underestimate mineralization in individual lesions. This is supported by our observations. Firstly, patients with a higher disease burden showed significantly greater changes in K_i than those with a low disease burden. Secondly, we observed an increase in metabolic activity in the non-metastatic skeleton at both trabecular and cortical sites, presumably as an effect of endocrine treatment. These changes were lower than those seen in metastases, so maintaining contrast between metastatic and normal skeleton, but were greater when measured by K_i than SUV parameters in cortical bone.

This study is limited by a relatively small number of patients and so statistical comparisons are limited but partly mitigated by a larger number of lesions (n=52). Whilst measurement of K_i shows advantages over SUV_{max}, false positives caused by the flare phenomenon remain a factor that must be considered, as previously described *(31-33)*. We observed > 25% increase in K_i in 5 of 32 lesions (in non-PD patients) that might be accounted for by this phenomenon. Nevertheless, the ability to predict PD or non-PD after 8 weeks of endocrine treatment remains good in this cohort, especially using K_i, where all 4/4 PD patients and 7/8 non-PD patients were correctly predicted and K_i was a significantly better discriminator of PD from non-PD. Some of the smaller metastases may be susceptible to partial volume error introducing potential bias, although we did not attempt to correct for this. Percentage change, rather than absolute values of parameters, was of primary interest and partial volume errors would have been similar for each parameter given that the same ROIs were used for calculations. The modified Patlak method used in this analysis makes corrections for ^{18}F-fluoride efflux from bone and so errors resulting from no direct measurement of backflow from bone mineral (k_4) would be minimal (*23*). The population input function used in our method was

derived from postmenopausal women and whilst these did not have metastatic breast cancer, they did not have any other known skeletal disease and had a similar mean age to our patient cohort (54.8 years and 50.4 years, respectively). In addition, it has previously been shown that precision errors in ^{18}F-fluoride PET skeletal static and kinetic parameters are relatively small (coefficient of variation 12-14%) (*34*) and generally less than the changes we observed in this series.

Prediction of PD is most important to the oncologist as this allows an earlier therapeutic transition to second or third line therapy whilst minimizing potential toxicity from ineffective treatment. Patients with either stable disease or partial/complete response would normally have treatment continued and so it is clinically relevant to include both stable and responder groups together in this analysis.

A "gold" standard for predicting treatment response in bone metastases is lacking in clinical practice. However, our clinical reference standard was made as robust as possible by utilizing standard clinical data (imaging, biochemistry, tumor markers and clinical features) in consensus by two oncologists blinded to the PET results and also with the time advantage of allowing assessment up to 24 weeks.

CONCLUSION

This study has shown that measurement of ^{18}F-fluoride metabolic flux (K_i) in breast cancer bone metastases, using static ^{18}F-fluoride PET/CT with venous blood sample counts, is feasible and may be more reliable in differentiating PD from non-PD than semi-quantitative SUV measures. In particular, observed accurate identification of PD is important and of clinical utility. These preliminary results deserve further prospective validation in larger patient groups under different therapy regimes.

ACKNOWLEDGEMENTS

The authors acknowledge financial support from the King's College London / University College London Comprehensive Cancer Imaging Centres funded by Cancer Research UK and Engineering and Physical Sciences Research Council in association with the Medical Research Council and the Department of Health (C1519/A16463), Breast Cancer Now (2012NovPR013), the Wellcome Trust EPSRC Centre for Medical Engineering at King's College

London (WT203148/Z/16/Z), the Royal College of Radiologists, Alliance Medical Ltd and the support of the National Institute of Health Research Clinical Research Network (NIHR CRN). We thank Dr Francois Cousin for his input in the study.

REFERENCES

1. Petrén-Mallmin M, Andréasson I, Ljunggren Ö, et al. Skeletal metastases from breast cancer: uptake of 18F-fluoride measured with positron emission tomography in correlation with CT. *Skelet Radiol*. 1998;27:72-76.

2. Schiepers C, Nuyts J, Bormans G, et al. Fluoride kinetics of the axial skeleton measured in vivo with fluorine-18-fluoride PET. *J Nucl Med*. 1997;38:1970-1976.

3. Messa C, Goodman WG, Hoh CK, et al. Bone metabolic activity measured with positron emission tomography and [18F]fluoride ion in renal osteodystrophy: correlation with bone histomorphometry. *J Clin Endocrinol Metab.* 1993;77:949-955.

4. Piert M, Zittel TT, Becker GA, et al. Assessment of porcine bone metabolism by dynamic. *J Nucl Med*. 2001;42:1091-1100.

5. Doot RK, Muzi M, Peterson LM, et al. Kinetic analysis of 18F-Fluoride PET images of breast cancer bone metastases. *J Nucl Med*. 2010;51:521-527.

6. Yu EY, Duan F, Muzi M, et al. Castration-resistant prostate cancer bone metastasis response measured by 18F-fluoride PET after treatment with dasatinib and correlation with progression-free survival: results from American College of Radiology Imaging Network 6687. *J Nucl Med*. 2015;56:354-360.

7. Guise TA, Mohammad KS, Clines G, et al. Basic mechanisms responsible for osteolytic and osteoblastic bone metastases. *Clin Cancer Res*. 2006;12:6213s-6216s.

8. Cook GJ, Parker C, Chua S, Johnson B, Aksnes AK, Lewington VJ. 18F-fluoride PET: changes in uptake as a method to assess response in bone metastases from castrate-resistant prostate cancer patients treated with 223Ra-chloride (Alpharadin). *EJNMMI Res*. 2011;1:4.

9. Blake GM, Frost ML, Fogelman I. Quantitative radionuclide studies of bone. *J Nucl Med*. 2009;50:1747-1750.

10. Blake GM, Siddique M, Frost ML, Moore AE, Fogelman I. Radionuclide studies of bone metabolism: do bone uptake and bone plasma clearance provide equivalent measurements of bone turnover? *Bone*. 2011;49:537-542.

11. Hawkins RA, Choi Y, Huang SC, et al. Evaluation of the skeletal kinetics of fluorine-18-fluoride ion with PET. *J Nucl Med*. 1992;33:633-642.

12. Cook GJ, Blake GM, Marsden PK, Cronin B, Fogelman I. Quantification of skeletal kinetic indices in Paget's disease using dynamic 18F-fluoride positron emission tomography. *J Bone Miner Res*. 2002;17:854-859.

13. Frost ML, Cook GJ, Blake GM, Marsden PK, Benatar NA, Fogelman I. A prospective study of risedronate on regional bone metabolism and blood flow at the lumbar spine measured by 18F-fluoride positron emission tomography. *J Bone Miner Res*. 2003;18:2215-2222.

14. Installe J, Nzeusseu A, Bol A, Depresseux G, Devogelaer JP, Lonneux M. (18)F-fluoride PET for monitoring therapeutic response in Paget's disease of bone. *J Nucl Med*. 2005;46:1650-1658.

15. Frost ML, Siddique M, Blake GM, et al. Differential effects of teriparatide on regional bone formation using (18)F-fluoride positron emission tomography. *J Bone Miner Res*. 2011;26:1002-1011.

16. Patlak CS, Blasberg RG. Graphical evaluation of blood-to-brain transfer constants from multiple-time uptake data. Generalizations. *J Cereb Blood Flow Metab*. 1985;5:584-590.

17. Brenner W, Vernon C, Muzi M, et al. Comparison of different quantitative approaches to 18F-fluoride PET scans. *J Nucl Med*. 2004;45:1493-1500.

18. Siddique M, Frost ML, Blake GM, et al. The precision and sensitivity of (18)F-fluoride PET for measuring regional bone metabolism: a comparison of quantification methods. *J Nucl Med*. 2011;52:1748-1755.

19. Cook GJ, Lodge MA, Marsden PK, Dynes A, Fogelman I. Non-invasive assessment of skeletal kinetics using fluorine-18 fluoride positron emission tomography: evaluation of image and population-derived arterial input functions. *Eur J Nucl Med Mol Imaging*. 1999;26:1424-1429.

20. Puri T, Blake GM, Siddique M, et al. Validation of new image-derived arterial input functions at the aorta using 18F-fluoride positron emission tomography. *Nucl Med Commun*. 2011;32:486-495.

21. Puri T, Blake GM, Frost ML, et al. Validation of image-derived arterial input functions at the femoral artery using 18F-fluoride positron emission tomography. *Nucl Med Commun*. 2011;32:808-817.

22. Chen K, Bandy D, Reiman E, et al. Noninvasive quantification of the cerebral metabolic rate for glucose using positron emission tomography, 18F-fluoro-2-deoxyglucose, the Patlak method, and an image-derived input function. *J Cereb Blood Flow Metab*. 1998;18:716-723.

23. Siddique M, Frost ML, Moore AE, Fogelman I, Blake GM. Correcting (18)F-fluoride PET static scan measurements of skeletal plasma clearance for tracer efflux from bone. *Nucl Med Commun*. 2014;35:303-310.

24. Blake GM, Siddique M, Puri T, et al. A semipopulation input function for quantifying static and dynamic 18F-fluoride PET scans. *Nucl Med Commun*. 2012;33:881-888.

25. Moore AE, Blake GM, Taylor KA, et al. Assessment of regional changes in skeletal metabolism following 3 and 18 months of teriparatide treatment. *J Bone Miner Res*. 2010;25:960-967.

26. Cook GJ, Lodge MA, Blake GM, Marsden PK, Fogelman I. Differences in skeletal kinetics between vertebral and humeral bone measured by 18F-fluoride positron emission tomography in postmenopausal women. *J Bone Miner Res*. 2000;15:763-769.

27. Siddique M, Blake GM, Frost ML, et al. Estimation of regional bone metabolism from whole-body 18F-fluoride PET static images. *Eur J Nucl Med Mol Imaging*. 2012;39:337-343.

28. Lecouvet FE, Talbot JN, Messiou C, Bourguet P, Liu Y, de Souza NM. Monitoring the response of bone metastases to treatment with Magnetic Resonance Imaging and nuclear medicine techniques: a review and position statement by the European Organisation for Research and Treatment of Cancer imaging group. *Eur J Cancer*. 2014;50:2519-2531.

29. Rohren EM, Etchebehere EC, Araujo JC, et al. Determination of skeletal tumor burden on 18F-Fluoride PET/CT. *J Nucl Med*. 2015;56:1507-1512.

30. Hunter JG, Hamberg LM, Alpert NM, Choi NC, Fischman AJ. Simplified Measurement of Deoxyglucose Utilization Rate. *J Nucl Med.* 1996;37:950-955.

31. Wade AA, Scott JA, Kuter I, Fischman AJ. Flare response in 18F-fluoride ion PET bone scanning. *Am J Roentgenol*. 2006;186:1783-1786.

32. Cook GJ, Taylor BP, Glendenning J, et al. Heterogeneity of treatment response in skeletal metastases from breast cancer in 18F-fluoride and 18F-FDG PET. *Nucl Med Commun*. 2015;36:515-516.

33. Cook GJ, Azad GK, Goh V. Imaging bone metastases in breast cancer: staging and response assessment. *J Nucl Med*. 2016;57 (Suppl 1):27s-33s.

34. Frost ML, Blake GM, Park-Holohan SJ, et al. Long-term precision of 18F-fluoride PET skeletal kinetic studies in the assessment of bone metabolism. *J Nucl Med*. 2008; 49: 700–707.

FIGURE 1

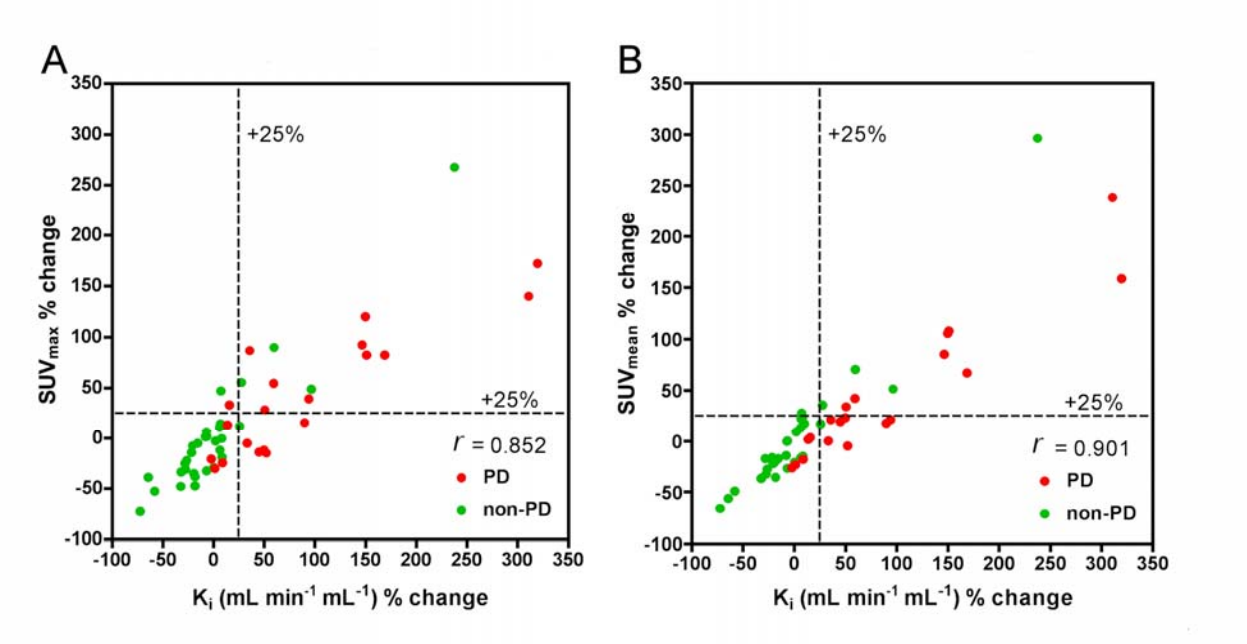

Lesion analysis: Scatter plot for percentage changes in K_i values against percentage changes in SUV_{max} and SUV_{mean}, for PD and non-PD, 8 weeks after the start of treatment

FIGURE 2

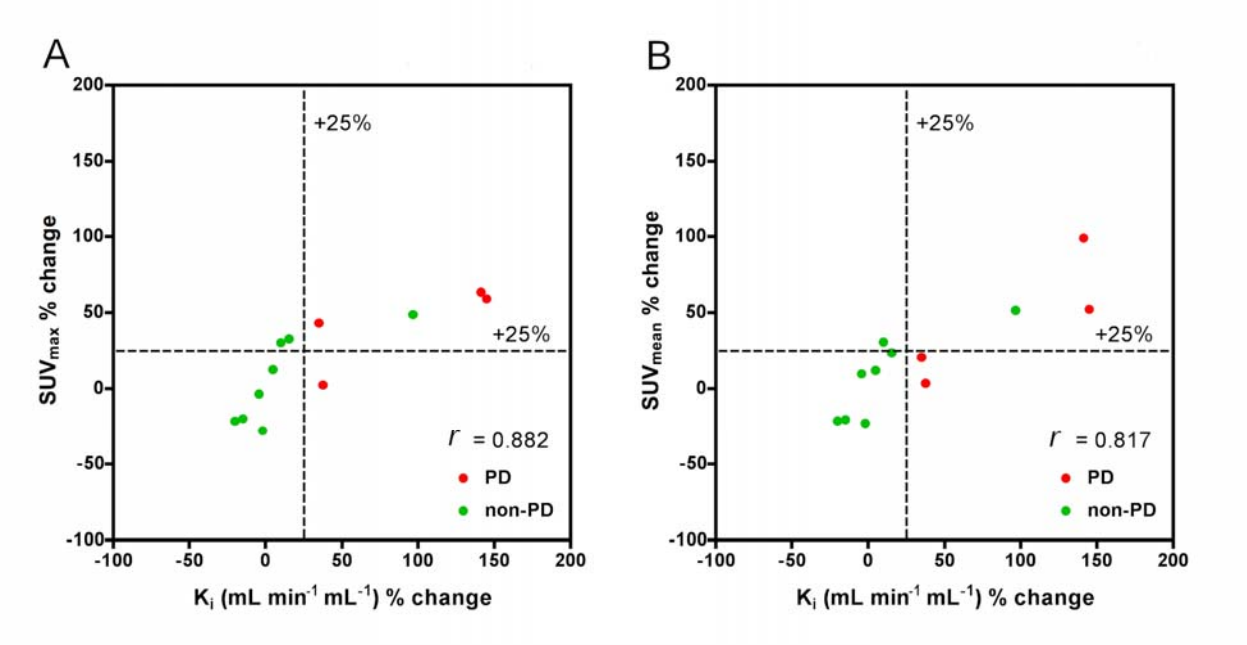

Patient basis: Scatter plot for percentage changes in K_i values against percentage changes in SUV_{max} and SUV_{mean} for PD and non-PD, 8 weeks after the start of treatment

TABLES

Table 1

Mean tumor volume, SUV_{mean} (g/mL), SUV_{max} (g/mL) and K_i (mL min^{-1} mL^{-1}) at baseline, 8 weeks and percentage change at 8 weeks

Lesions (n=52) at baseline				**Lesions (n=52) at 8 weeks**				**% change at 8 weeks**		
Tumor volume ($cm^{3)}$	K_i (mL min^{-1} mL^{-1})	SUV_{max} (g/mL)	SUV_{mean} (g/mL)	Tumor volume (cm^3)	K_i (mL min^{-1} mL^{-1})	SUV_{max} (g/mL)	SUV_{mean} (g/mL)	K_i (mL min^{-1} mL^{-1})	SUV_{max} (g/mL)	SUV_{mean} (g/mL)
6.8	0.067	35.1	18.8	6.6	0.08	38.3	20.8	34.9	16.1	17.5

Table 2

Comparison of correlation coefficients between changes in K_i (mL min^{-1} mL^{-1}), SUV_{max} (g/mL) and SUV_{mean} (g/mL) after 8 weeks of endocrine therapy in 12 patients (52 lesions). (PD – progressive disease)

	Correlation coefficient *r* (p value) at baseline	**Correlation coefficient *r* (p value) at 8 weeks**	**Correlation coefficient *r* (p value) % change at 8 weeks after treatment**	**Correlation coefficient *r* (p value) % change in patients with PD**	**Correlation coefficient *r* (p value) % change in patients with non-PD**
K_i (mL min^{-1} mL^{-1}) Vs SUV_{max} (g/mL)	0.632 (p<0.001)	0.830 (p<0.001)	0.852 (p<0.001)	0.811 (p<0.001)	0.863 (p<0.001)
K_i (mL min^{-1} mL^{-1}) Vs SUV_{mean}(g/mL)	0.784 (p<0.001)	0.901 (p<0.001)	0.901 (p<0.001)	0.904 (p<0.001)	0.933 (p<0.001)

Table 3

Comparison of PD (4 patients, 20 lesions) and non-PD (8 patients, 32 lesions): mean K_i (mL min^{-1} mL^{-1}), SUV_{max} (g/ml) and SUV_{mean} (g/ml) at baseline, 8 weeks and percentage change at 8 weeks for the lesions in individual subjects

	Patient	**Baseline**			**8 weeks**			**% change at 8 weeks**		
		K_i (mL min^{-1} mL^{-1})	SUV_{max} (g/mL)	SUV_{mean} (g/mL)	K_i (mL min^{-1} mL^{-1})	SUV_{max} (g/mL)	SUV_{mean} (g/mL)	K_i (mL min^{-1} mL^{-1})	SUV_{max} (g/mL)	SUV_{mean} (g/mL)
PD	1	0.033	25.7	12.0	0.075	37.1	16.9	144.9	58.9	52.1
	2	0.071	32.6	20.2	0.091	32.6	19.6	37.6	2.3	3.5
	3	0.047	49.6	21.9	0.121	85.9	46.8	141.2	63.3	98.9
	4	0.083	30.7	19.4	0.110	44.0	23.1	35.1	43.1	20.6
Non-PD	1	0.067	25.8	11.7	0.063	25.74	12.72	-4.3	-3.7	9.7
	2	0.145	60.9	34.4	0.121	46.96	26.64	-14.8	-19.9	-20.6
	3	0.078	37.6	21.7	0.076	26.70	16.72	-1.9	-28.0	-23.0
	4	0.045	38.8	19.8	0.036	30.38	15.47	-20.1	-21.6	-21.5
	5	0.051	26.1	14.4	0.051	27.35	15.40	4.8	12.5	11.9
	6	0.040	12.4	25.3	0.079	37.59	18.77	96.7	48.7	51.4
	7	0.055	25.0	14.8	0.063	34.73	18.31	15.4	32.7	23.5
	8	0.059	27.6	13.4	0.051	23.68	14.02	10.1	30.1	30.5
P value PD vs non-PD								P=<0.01	P=0.067	P=0.153

Supplementary data 1:

Detailed methodology for K_i calculation

The measurement of ^{18}F-fluoride metabolic flux (K_i, also referred to as ^{18}F skeletal plasma clearance) provides a more reliable assessment of bone metabolism than standardized uptake values (SUV) in circumstances where bone metabolism averaged across the whole skeleton is sufficiently different from normal that the ^{18}F plasma time-activity curve (TAC) is altered. Examples may include patients with extensive metastatic bone disease ("super scans"), patients with an extensive area of active Paget's disease, and patients with osteoporosis treated with a potent anabolic bone agent such as teriparatide *(1-3)*. In such cases the increased avidity of ^{18}F uptake into bone leaves less tracer available for the circulation or for uptake in soft tissue and the ^{18}F concentration in plasma is correspondingly reduced. The ^{18}F-fluoride semi-population input function (SPIF) was developed so that when combined with a single static PET scan acquired 45 to 90 minutes after injection of tracer it provides a quick and simple method of estimating K_i with little loss of accuracy or precision compared with the conventional 60-minute dynamic PET scan analyzed with an input function generated by continuous arterial sampling *(4-6)*. An important advantage of this approach is that it enables measurements of K_i to be made at multiple sites in the skeleton at different bed positions with only a single injection of ^{18}F-fluoride tracer. In the SPIF method the "terminal exponential" is defined as the single-exponential curve fitted to between two and four measurements of ^{18}F venous plasma concentration between 30 and 90 minutes after injection *(4).* At times greater than 30 minutes ^{18}F concentrations in venous and arterial blood are in equilibrium and equal. In the example from the present study shown in Figure S1A, two blood samples were taken at 55 and 85 minutes after injection with plasma concentration measurements of 7.21 and 5.06 kBq/mL after decay correction to the time of injection. The injected activity in this subject was 237 MBq. To generate an estimate of the full plasma TAC between 0 and 90 minutes after injection the terminal exponential calculated from the 55 and 85 minute blood samples is added to a "residual"

curve (Figure S1B) representing the bolus peak and early fast exponentials. The residual curve shown in Figure S1B was produced by averaging data from 10 postmenopausal women who had full arterial blood sampling between 0 and 60 minutes after injection with subtraction of the terminal exponential *(4).* The residual curve in each of the 10 women was normalised to an injected activity of 100 MBq, and the curves averaged after adjusting the time of peak counts to 30 seconds after initiation of the injection protocol. The full SPIF TAC (Figure S1C) was created by multiplying the residual curve by 2.37 (allowing for the injected activity of 237 MBq in this instance) and adding the terminal exponential shown in Figure S1A. To ensure that the contribution from the terminal exponential does not exceed the residual curve in the first 30 seconds after injection the terminal exponential in Figure S1A was rolled off to zero using a ramp function at times before 30 seconds *(4).*

In the example shown in Figure S1C, the terminal exponential accounts for over 80% of the area under the curve between 0 and 90 minutes. The contribution from the terminal exponential exceeds the contribution from the residual curve at times greater than 3 minutes after injection. An important part of the rationale for the SPIF method is that changes in the whole skeleton metabolic flux may alter the terminal exponential, but will have less effect on the residual curve, which is mainly determined by the mixing of the bolus injection throughout the circulation and the rapid early diffusion of ^{18}F-fluoride ions into soft tissue.

In the analysis of conventional 60-minute ^{18}F-fluoride dynamic PET scans, the metabolic flux K_i is often calculated from the bone TAC and the arterial input function using the Hawkins compartmental model (Figure S2) *(7).* However, provided that the rate constant k_4 describing the efflux of tracer out of the bound bone pool is negligibly small, the alternative Patlak analysis method provides a simpler method of calculating K_i from the dynamic scan data. In Patlak analysis the concentration of ^{18}F in the bone region of interest, $C_b(T)$, at time T after injection is expressed by the following equation:

$$\frac{C_b(T)}{C_p(T)} = V + K_i \frac{\int_0^T C_p(t)dt}{C_p(T)} \quad (1)$$

where C_p is the concentration of tracer in plasma and the intercept of the straight line, V, is the volume of distribution in the unbound bone pool (Figure S2). To allow for equilibration between tracer in plasma and the unbound bone pool in the first 10 minutes after injection, the values of K_i and V are determined by fitting a straight line to the 10-60 minute data *(5).*

In practice, the assumption that k_4 is negligibly small is not strictly valid. As a consequence the points of the Patlak plot deviate from the straight-line relationship of Equation 1, and as a result the K_i results underestimate the Hawkins model values. This problem is avoided by using a modified Patlak analysis that introduces a rate constant k_{loss} to represent the efflux of tracer out of the bound bone pool into plasma *(8).* Following the method described by Holden et al. *(9)*, Equation 1 is rewritten as:

$$\frac{C_b(T)}{C_p(T)} = V + K_i\theta(T) \quad (2a)$$

where: $$\theta(T) = \frac{\int_0^T C_p(t)\exp(-k_{loss}(T-t))\,dt}{C_p(T)} \quad (2b)$$

In this modified analysis the rate constant k_{loss} is varied until the plot of normalized activity $\frac{C_b(T)}{C_p(T)}$ against normalized time $\theta(T)$ from 10-60 minutes after injection gives the best fit to a straight line *(8).* Siddique et al. applied the Holden method to 60-minute dynamic PET scans of the spine and hip and reported mean values of k_{loss} ~0.006 min^{-1} at both sites along with mean values for the volume of distribution V of around 0.2 in the spine and 0.1 in the hip *(8).*

In Siddique's method, the measurement of K_i is made by combining the semi-population input function with measurements of regional bone uptake from a series of short static PET scans acquired at multiple

bed positions between 45 and 90 minutes after injection *(5,8).* The value of K_i is found from a simplified Patlak plot consisting of just two data points, representing the measured tracer concentration in the bone region of interest at the time *T* of the static scan and the population mean value of the intercept *V.* Rearranging Equation 2a we have:

$$K_i = \frac{\frac{C_b(T)}{C_p(T)} - V}{\theta(T)} \qquad (3)$$

K_i is calculated from Equation 3 using the population mean values of *V* and the efflux rate constant k_{loss} *(8,10).*

Acknowledgement

The authors are grateful to Dr Tanuj Puri for creating Figure S2.

References

1. Blake GM, Zivanovic MA, McEwan AJ, Ackery DM. ^{89}Sr therapy: strontium kinetics in disseminated carcinoma of the prostate. *Eur J Nucl Med.* 1986;12:447-54.
2. Gnanasegaran G, Moore AE, Blake GM, Vijayanathan S, Clarke SE, Fogelman I. Atypical Paget's disease with quantitative assessment of tracer kinetics. *Clin Nucl Med*. 2007;32:765-9.
3. Blake GM, Siddique M, Frost ML, Moore AE, Fogelman I. Radionuclide studies of bone metabolism: Do bone uptake and bone plasma clearance provide equivalent measurements of bone turnover? *Bone*. 2011;49:537-42.
4. Blake GM, Siddique M, Puri T, et al. A semipopulation input function for quantifying static and dynamic ^{18}F-fluoride PET scans. *Nucl Med Commun*. 2012;33:881-8.
5. Siddique M, Blake GM, Frost ML, et al. Estimation of regional bone metabolism from whole-body ^{18}F-fluoride PET static images. *Eur J Nucl Med Mol Imaging*. 2012;39:337-43.
6. Siddique M, Frost ML, Blake GM, et al. The precision and sensitivity of ^{18}F-fluoride PET for measuring regional bone metabolism: a comparison of quantification methods. *J Nucl Med.* 2011;52:1748-55.
7. Hawkins RA, Choi Y, Huang SC, et al. Evaluation of the skeletal kinetics of fluorine-18-fluoride ion with PET. *J Nucl Med*. 1992;33:633-42.
8. Siddique M, Frost ML, Moore AE, Fogelman I, Blake GM. Correcting ^{18}F-fluoride PET static scan measurements of skeletal plasma clearance for tracer efflux from bone. *Nucl Med Commun*. 2014;35:303-10.
9. Holden JE, Doudet D, Endres CJ, et al. Graphical analysis of 6-fluoro-L-dopa trapping: effect of inhibition of catechol-O-methyltransferase. *J Nucl Med*. 1997; 38:1568-74.
10. Blake GM, Puri T, Siddique M, Frost ML, Moore AEB, Fogelman I. Site specific measurements of bone formation using ^{18}F-sodium fluoride PET/CT. *Quant Imaging Med Surg*. 2018;8:47-59.

Supplemental Figure Legends

FIGURE S1

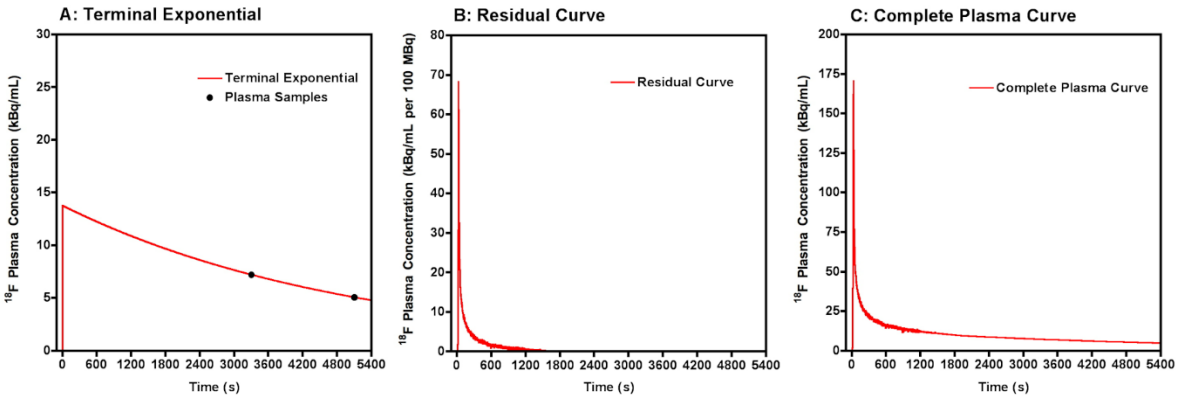

A) ^{18}F-fluoride plasma concentration curve showing timing of 55 and 85 minute blood samples used to calculate the terminal exponential.

B) Residual ^{18}F-fluoride plasma concentration curve derived from 10 post menopausal women.

C) Resultant full ^{18}F-fluoride plasma concentration curve.

FIGURE S2

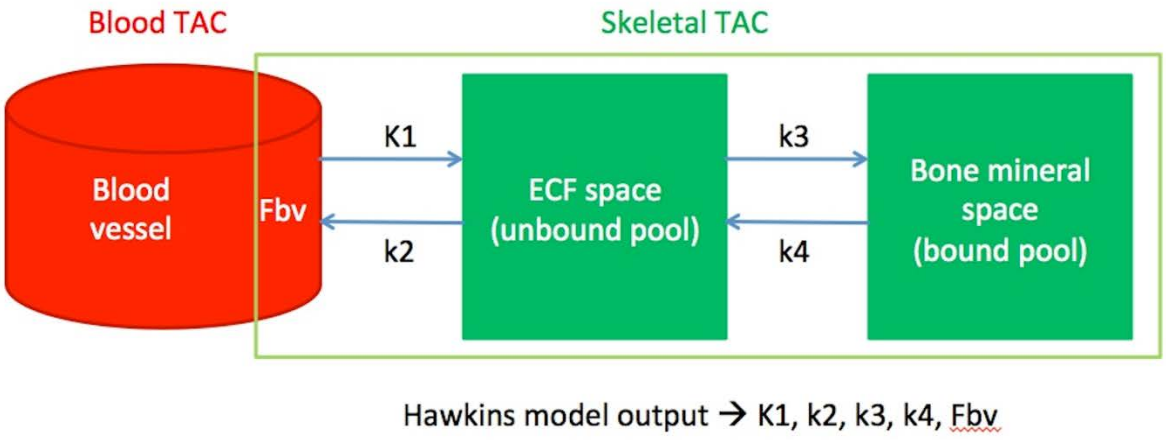

Illustration of the compartmental model describing ^{18}F-fluoride kinetics in bone

Supplementary data 2:

	Lesions (n=52) at baseline				Lesions (n=52) at 8 weeks				% change at 8 weeks			
Patient	Tumor volume (cm^3) baseline	K_i (mL min^{-1} mL^{-1})	SUV_{max} (g/mL)	SUV_{mean} (g/mL)	Tumor volume (cm^3) 8 weeks	K_i (mL min^{-1} mL^{-1})	SUV_{max} (g/mL)	SUV_{mean} (g/mL)	K_i (mL min^{-1} mL^{-1})	SUV_{max} (g/mL)	SUV_{mean} (g/mL)	Clinical reference standard
1	5.9	0.041	28.7	14.7	5.3	0.080	39.9	17.8	95.1	39.0	21.1	PD(CT,BS, ALP,PS)
	4.0	0.029	23.4	10.6	3.8	0.079	42.7	17.7	172.4	82.5	67.0	
	12.9	0.047	42.0	16.9	13.1	0.072	35.8	16.1	53.2	-14.8	-4.7	
	5.2	0.025	16.3	9.1	3.6	0.048	18.8	10.7	92.0	15.3	17.6	
	1.8	0.024	17.8	8.6	1.7	0.099	48.4	22.2	319.6	172.1	158.8	
2	10.3	0.057	32.4	16.3	5.1	0.141	62.2	30.1	147.4	92.0	84.7	PD(CT,BS,ALP,PS)
	2.9	0.076	31.0	21.7	3.7	0.075	24.5	16.0	-1.3	-21.0	-26.3	
	3.2	0.034	18.4	9.9	10.1	0.046	17.4	9.9	35.3	-5.4	0.0	
	5.1	0.100	41.0	28.6	6.9	0.109	30.9	23.4	9.0	-24.6	-18.2	
	12.7	0.085	40.3	24.3	18.7	0.087	28.1	18.6	2.4	-30.3	-23.5	
3	18.1	0.032	30.6	15.0	3.7	0.048	26.9	18.4	49.8	-11.8	23.4	PD(CT,ALP,TM,PS)
	9.5	0.076	74.0	35.5	11.2	0.192	134.7	73.7	152.6	82.0	107.6	
	6.7	0.040	38.9	18.6	11.7	0.099	85.5	38.1	147.5	119.8	104.8	
	10.3	0.055	60.1	25.5	9.2	0.224	144.3	86.1	307.3	140.1	237.6	
	12.1	0.032	44.3	14.9	18.8	0.046	38.1	17.8	44.8	-13.7	19.4	
4	4.8	0.053	21.7	12.4	1.4	0.080	27.8	16.6	50.9	28.1	33.9	PD(CT,BS, ALP,PS)
	5.5	0.094	34.6	21.9	5.5	0.107	39.1	22.3	13.8	13.0	1.8	
	7.4	0.089	32.9	20.8	8.5	0.103	43.8	21.5	15.7	33.1	3.4	
	3.5	0.088	34.2	20.6	1.7	0.140	52.7	29.2	59.1	54.1	41.7	
	4.4	0.091	30.3	21.2	2.0	0.123	56.6	25.7	35.2	86.8	21.2	
5	4.7	0.068	24.8	11.9	3.3	0.049	18.4	9.8	-27.9	-25.8	-17.6	Non-PD(CT,BS,ALP,TM,PS)
	2.3	0.103	41.3	17.9	2.5	0.110	47.2	21.9	6.8	14.3	22.3	
	4.8	0.029	11.5	5.1	3.2	0.031	11.4	6.3	6.9	-0.9	23.5	
6	11.4	0.172	70.6	40.8	10.6	0.125	48.5	27.5	-27.3	-31.3	-32.6	Non-PD (CT,BS,ALP,PS)
	32.7	0.133	57.3	31.6	25.6	0.168	64.2	37.0	26.3	12.0	17.1	
	6.6	0.140	67.7	33.1	2.5	0.095	35.2	20.9	-32.1	-48.0	-36.9	
	2.8	0.104	41.6	24.7	6.0	0.096	42.1	21.2	-7.7	1.2	-14.2	
	17.9	0.176	67.4	41.8	17.9	0.120	44.6	26.4	-31.8	-33.8	-36.8	

7	5.8	0.094	42.2	26.3	6.7	0.095	29.9	20.7	1.1	-29.1	-21.3	Non-PD(CT,ALP,PS)
	3.0	0.060	27.4	16.9	3.1	0.066	22.1	14.4	10.0	-19.3	-14.8	
	5.6	0.083	38.5	23.2	6.5	0.089	33.9	19.4	7.2	-11.9	-16.4	
	6.2	0.077	43.7	21.6	6.1	0.063	23.0	13.9	-18.2	-47.4	-35.6	
	6.3	0.074	36.3	20.6	5.4	0.069	24.5	15.0	-6.8	-32.5	-27.2	
8	2.9	0.047	44.7	20.5	2.9	0.038	29.0	16.2	-19.1	-35.1	-21.0	Non-PD (CT,BS,ALP,TM,PS)
	2.5	0.046	37.0	20.3	4.0	0.039	35.1	16.7	-15.2	-5.1	-17.7	
	2.9	0.049	43.7	21.4	5.9	0.036	34.1	15.4	-26.5	-22.0	-28.0	
	2.5	0.051	36.7	22.6	3.0	0.041	33.9	17.6	-19.6	-7.6	-22.1	
	2.3	0.032	31.9	14.0	1.8	0.026	19.6	11.2	-18.8	-38.6	-20.0	
9	2.2	0.062	33.9	17.4	2.8	0.064	32.9	19.0	3.2	-2.9	9.2	Non-PD (CT,BS,PS)
	5.0	0.046	25.9	12.9	3.9	0.051	29.2	15.1	10.9	12.7	17.1	
	1.8	0.081	40.5	22.5	2.2	0.064	34.7	18.9	-21.0	-14.3	-16.0	
	3.4	0.030	15.3	8.6	4.4	0.032	17.0	9.6	6.7	11.1	11.6	
	1.3	0.037	14.7	10.5	2.4	0.047	22.8	14.2	27.0	55.1	35.2	
10	12.7	0.040	25.3	12.4	9.9	0.079	37.5	18.7	97.5	48.2	50.8	Non-PD (CT,BS,ALP,PS)
11	6.3	0.069	29.2	18.6	6.1	0.065	29.7	18.6	-5.8	1.7	0.0	Non-PD (BS,ALP,TM,PS)
	5.5	0.055	30.9	14.9	5.6	0.088	58.6	25.3	60.0	89.6	69.8	
	1.3	0.040	14.8	11.0	1.3	0.037	15.7	10.9	-7.5	6.1	-0.9	
12	21.4	0.067	45.1	15.3	22.8	0.019	12.4	5.2	-71.6	-72.5	-66.0	Non-PD(CT,BS,ALP,PS)
	10.7	0.049	23.0	11.3	8.4	0.018	14.0	4.9	-63.3	-39.1	-56.6	
	2.8	0.038	12.7	8.8	2.0	0.129	46.8	34.7	239.5	268.5	294.3	
	2.1	0.052	18.2	11.8	2.0	0.055	26.7	15.0	5.8	46.7	27.1	
	8.5	0.088	38.9	20.0	9.2	0.037	18.3	10.1	-58.0	-53.0	-49.5	
Mean	6.8	0.067	35.1	18.8	6.6	0.08	38.3	20.8	35.1	16.0	17.2	

SUV_{mean} (g/ml), SUV_{max} (g/ml) and K_i (mL min^{-1} mL^{-1}) at baseline, 8 weeks, percentage change and mean percentage change at 8 weeks in patients with progressive disease (PD) and non-progressive disease (non-PD)

PS pain score, BS bone scan, CT computed tomography, ALP alkaline phosphatase, TM tumor marker